PCCP

Achieving optimum carrier concentrations in $p-$doped SnS thermoelectrics

Journal:	*Physical Chemistry Chemical Physics*
Manuscript ID:	CP-ART-12-2014-005991.R1
Article Type:	Paper
Date Submitted by the Author:	29-Jan-2015

Complete List of Authors:	Bhattacharya, Sandip; Ruhr University Bochum, Interdisciplinary Centre for Advanced Materials Simulation (ICAMS) Gunda, N. S. Harsha; Ruhr University Bochum, Interdisciplinary Centre for Advanced Materials Simulation (ICAMS) Stern, Robin; Ruhr University Bochum, Interdisciplinary Centre for Advanced Materials Simulation (ICAMS) Jacob, Stephane; IMRA Europe S.A.S., Chmielowski, Radoslaw; IMRA Europe S.A.S., DENNLER, Gilles; IMRA Europe S.A.S., ; IMRA Europe, Madsen, Georg; Ruhr University Bochum, Interdisciplinary Centre for Advanced Materials Simulation (ICAMS); Ruhr University Bochum,

CREATED USING THE RSC LaTeX PCCP ARTICLE TEMPLATE – SEE www.rsc.org/electronicfiles FOR DETAILS

ARTICLE TYPE www. rsc.org/xxxxxx | XXXXXXXX

Achieving optimum carrier concentrations in $p-$doped SnS thermoelectrics

Sandip Bhattacharya,*[a] N. S. Harsha Gunda,[a], Robin Stern[a], Stéphane Jacobs[b], Radoslaw Chmielowski[b], Gilles Dennler [b] and Georg K. H. Madsen[a]

Received Xth XXXXXXXXXX 20XX, Accepted Xth XXXXXXXXX 20XX

First published on the web Xth XXXXXXXXXX 200X

DOI: 10.1039/b000000x

Tin(II)sulfide, SnS, is a commercially viable and environmentally friendly thermoelectric material. Recently it was shown how the carrier concentration and thermoelectric power factor can be optimized by Ag-doping under a sulphur rich environment. Theoretical calculations lead to a fairly accurate estimation of the carrier concentration, whereas the potential of doping with Li^+ is strongly overestimated. Two principally ubiquitous effects that can result in decreasing the hole concentration, namely the formation of coupled defect complexes and oxidation of the dopant, are discussed as possible origin of this disagreement. It is shown that oxidation limits the chemical potential of Li beyond that already set by the formation of Li_2S. This work serves as a comprehensive guide to achieve an efficient $p-$doped SnS thermoelectric material.

Tin(II)sulfide, SnS, is a promising thermoelectric material. It exhibits low thermal conductivity [1], possesses an electronic band structure indicating favorable transport properties [2] and the carrier concentration can be controlled by extrinsic doping. [3] Furthermore, it serves as an enticing candidate for thermoelectric power generation because of the abundant availability of its constituents and ease of manufacturing large quantities of it commercially. However, undoped SnS has a large resistivity, $\rho \geq 10$ Ωcm, [4] due to a concentration of charge carriers of only $n \approx 10^{16}$ cm^{-3}. [5–7] Recently we performed a high-throughput first-principles study of extrinsic defects in SnS [3] aimed at exploring the different $p-$dopants that could potentially enhance the carrier concentration in SnS. This indicated monovalent cations as potential doping candidates to optimize the fraction of itinerant holes in SnS. Subsequent synthesis by spark plasma sintering (SPS) confirmed Ag^+ doped SnS, to have an electrical resistivity ($\rho = 38$ mΩcm at $T = 330$ K) almost an order of magnitude lower than previously obtained. [3] Correspondingly, a Seebeck coefficient of $S = 275$ μV/K and a power factor of PF= 199 μW m^{-2} K^{-2} were measured at 330 K. [3] The results were confirmed by Tan *et al*. [8] They also performed Hall measurements finding carrier concentrations around $2.7-3.6\times10^{18}$ cm^{-3}, in good agreement with the theoretical predictions. [3] Preliminary experiments for Li_2S doped SnS were also performed, but no $\rho < 200$ mΩcm was found. This is quite surprising considering the otherwise good agreement between experiment and theory and the fact that our theoretical predictions found the Li_{Sn} defect to be energetically more favorable than Ag_{Sn}. [3]

In this paper we explore the origin behind the discrepancy between experiments and theory. We experimentally confirmed that Li doping of SnS led to a low carrier concentration, even when grown in ultra-high vacuum. We then investigated theoretically the effects of two prevalent mechanisms that could affect the doping of SnS. First we considered the formation of coupled defects. Such defects result from a formation of a stable agglomerate of individual point defects due to their binding energy being large compared to the formation energies of the individual defects. In certain circumstances coupled defects have been argued to play an important role. One example is Li doped ZnO where the hole-doping substitutional Li_{Zn} defect is compensated by a coupled interstitial Li_{Int} defect. [9] Another example is the unusual $n-$type conductivity of $CoSb_3$, which can be explained by the formation of Co_{Int} defect pairs. [10] However, for Li:SnS we did not find coupled Li defects as a viable explanation of the low carrier concentration. We then considered the possibility of oxidation of the dopants and found that, despite the presence of Li_2S and UHV conditions, the formation of Li_2O does indeed limit the chemical potential of Li.

1 Experimental results

All the pristine and doped SnS samples have been prepared and measured following the same procedure. SnS powders have been purchased from Sigma Aldrich with a 96% purity guaranteed on the metal base. Prior to any experiment, the phase purity of the powder was verified by X-Ray Diffraction (D8, Brucker). This step appeared mandatory as we ob-

[a] *ICAMS, Ruhr-Universität Bochum, 44780 Bochum, Germany; E-mail: sandip.bhattacharya@rub.de*

[b] *IMRA Europe S.A.S., 06904 Sophia Antipolis, France.*

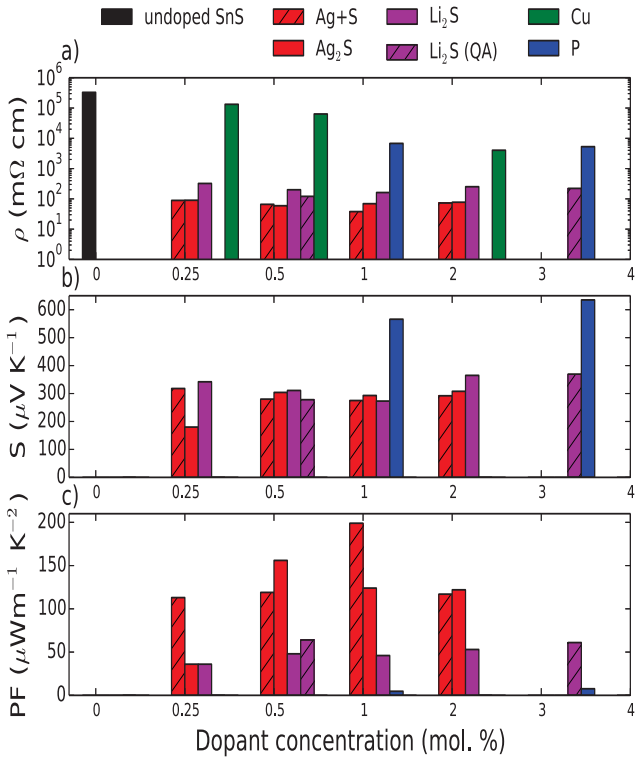

Fig. 1 Measured (a) Resistivity, (b) Seebeck coefficient and (c) Power factor of SnS doped with various dopants for the SPS experiments ($p^{SPS} = 2.1 \times 10^{-3}$ Pa). Additionally, Li_2S doped SnS samples were prepared under UHV conditions in quartz ampules ($p^{QA} = 1 \times 10^{-8}$ Pa). Certain dopants at low concentrations resulted in very large resistivities, so that measuring S became impossible. These correspond to the missing bars in the transport measurements.

served a significant batch-to-batch variation in the fine composition of the powders. Indeed, some of the lots were found to comprise a non-negligible amount of SnS_2 and/or Sn_2S_3. The powders were poured in a graphite dye with an inner diameter of 10mm. Pellets were then fabricated by SPS (SPS-211Lx, Fuji Electronic Industrial Co. Ltd.) by applying a pressure of 50 MPa at a temperature of 550°C. The whole SPS sequence lasted 480 s. The densities of all the samples reported herein were above 90%, as measured by the Archimedes method. The ambient pressure in these particular experiments was 2.1×10^{-3} Pa.

In order to dope the sample, we added to the SnS powder, prior to the SPS step, a given amount of dopant taken from Ag, Cu, S, Li_2S, Ag_2S and P. All dopants were purchased in 5N quality (99.999% purity) and the matrix/dopant powder mixture were all prepared in a nitrogen glove-box. The mixture was then reacted either by SPS process, same as for the pristine powders, or by quartz ampoule (QA) approach. For the latter, the mixture was poured in a quartz ampoule. N_2 was evacuated from the QA until a pressure of 1×10^{-8} Pa is reached. The quartz ampoule was then sealed and placed in a vertical furnace (GSL-1100X2-VF, MTI corp.). The ampoule was heated from room temperature to 975°C at a rate of ≈ 2°C/min, dwelled at 975°C for 3 hours, cooled to 650 °C at a rate of ≈ 2 °C/min and quenched in a water bath. An ingot was recovered which was ground in an agate mortar. The resulting powder was passed through a sieve having a mesh with an opening of 150 μm. A pellet was finally prepared by sintering the sieved powder by SPS process.

The resistivity (ρ) and Seebeck coefficient (S), were both determined with a LSR-3 (Linseis GmbH) at a temperature of 330K. The measured ρ, S and power factor (PF) are schematically illustrated in Fig. 1. In the case of pristine SnS, a resistivity of 300 Ωcm was recorded. This value compares well with previous results published in the literature and indicates the necessity to dope the host material. Note that for undoped SnS, measuring S was not possible due to the large resistivity of the samples.

Doping SnS with Ag resulted in a minimum resistivity of $\rho = 38$ mΩcm and a PF= 199 μWm^{-1}K^{-2} for Ag+S concentration of 1 mol%. Along the same line, we have used Ag_2S as a dopant. This was also found to be soluble in the SnS host and reducing its resistivity thereby allowing us to obtain a max PF of 156 μWm^{-1}K^{-2}.

Motivated by the otherwise good agreement with the theoretical prediction and the fact that the Li_{Sn} defect was calculated to be more stable than the Ag_{Sn}[3], we tried to dope SnS using Li_2S. However, to our surprise, we measured high resistivities, with $\rho = 162$ mΩcm and $\rho = 121$ mΩcm as the lowest for the SPS and QA experiments respectively. These large resistivities resulted in maximum PF= 48 μWm^{-1}K^{-2} for SPS experiments and PF= 64 μWm^{-1}K^{-2} for QA experiments.

We furthermore tested P and Cu as dopants. In agreement with the predicted defect energy[3] we found comparably high resistivities when using P. While the defect energy of Cu_{Sn} was found to be marginally higher than Ag_{Sn},[3] it is not enough to explain that the resistivity of the Cu doped samples were almost an order of magnitude larger than the resistivity of the Ag doped samples.

2 Computational methodology

The procedure to evaluate the defect stability in the dilute limit from ab-initio calculations is quite well established.[11] The energy required to generate a defect, D, with charge q under given crystal growth condition is given as

$$E_d(D^{(q)}, \mu_e) = E_f(D^{(q)}) + q\mu_e - \sum_\alpha n_\alpha \Delta\mu_\alpha. \quad (1)$$

Here, $E_{\rm f}(\mathrm{D}^{(q)}) = E(\mathrm{D}^{(q)}) - E_{\rm bulk} - \sum_\alpha n_\alpha E_\alpha$ is the defect formation energy expressed with respect to its reference state. $E(\mathrm{D}^{(q)})$ is the total energy of the supercell containing the defect and $E_{\rm bulk}$ is the energy of the host material. Furthermore, n_α is the number of atoms of element α that are transferred to the defected cell from the reservior, E_α is the energy of the reference state and $\Delta\mu_\alpha$ is their corresponding chemical potentials. The chemical potential of the charge, $\mu_{\rm e}$, is given with respect to the valence band maximum (VBM).

The range of chemical potentials of the constituent atoms, $\Delta\mu_\alpha$, is controlled by the competing phases

$$\Delta\mu_{\rm Sn} \leq 0,\ \ \Delta\mu_{\rm S} \leq 0,\ \ \Delta\mu_{\rm Sn} + 2\Delta\mu_{\rm S} \leq 3\Delta H_{\rm f}(\mathrm{SnS_2}), \qquad (2)$$

Additionally, to grow the host SnS under thermodynamically equilibrium conditions we have the following requirement,

$$\Delta\mu_{\rm Sn} + \Delta\mu_{\rm S} = 2\Delta H_{\rm f}(\mathrm{SnS}). \qquad (3)$$

$\Delta H_{\rm f}$ appearing in Eq.(2) and Eq.(3) is the enthalpy of formation of the particular compound. In addition to these, the competing binary and ternary phases of the individual dopants with Sn and S, have also been accounted for in our calculations.

This procedure introduces an additional chemical potential of the dopant, $\Delta\mu_{\rm D}$. For D=Li the chemical potential of Li is limited by the formation of $\mathrm{Li_2S}$[3]

$$2\Delta\mu_{\rm Li} + \Delta\mu_{\rm S} \leq 3\Delta H_f(\mathrm{Li_2S}). \qquad (4)$$

One possible explanation of the high resistivity, measured when SnS is doped with $\mathrm{Li^+}$, is that $\mathrm{Li_{Sn}}$ defects are inhibited due to the oxidation of Li. In terms of Eq. (1) this translates into a lithium-oxide setting a stricter limit on the chemical potential of Li than that set by $\mathrm{Li_2S}$. The most commonly occurring and thermodynamically stable Li oxide is $\mathrm{Li_2O}$, and the relevant limit to the chemical potentials is:

$$2\,\Delta\mu_{\rm Li} + \Delta\mu_{\rm O} \leq 3\Delta H_f(\mathrm{Li_2O}). \qquad (5)$$

Here $\Delta\mu_{\rm O}$ is the chemical potential of oxygen. For gases, the pressure and temperature dependence of the chemical potential can be obtained from the well known expression for ideal gases[12–14]:

$$\Delta\mu_{\rm O}(T,p) = \Delta\mu_{\rm O}(T,p^o) + \frac{1}{2}\,k_B T\,\ln\left(\frac{p}{p^0}\right), \qquad (6)$$

where p^0 is the pressure at a reference state (in our calculations atmospheric pressure), p is the partial pressure of oxygen in our experiments, which is $p^{\rm QA} = 1\times10^{-8}$ Pa and $p^{\rm SPS} = 2.1\times10^{-3}$ Pa. Note that 1 atm is 101.325×10^3 Pa. Furthermore, given that the energy of the oxygen reference state is set to zero in calculating the formation energy of the oxide, Eq. (5), the temperature dependence of the chemical potential at a particular reference pressure, $\Delta\mu_{\rm O}(T,p^0)$, is given as

$$\begin{aligned}\Delta\mu_{\rm O}(T,p^0) =& \frac{1}{2}[H_{\rm O_2}(T,p^0) - H_{\rm O_2}(0K,p^0)] \\ &- \frac{1}{2}T[S_{\rm O_2}(T,p^0) - S_{\rm O_2}(0K,p^0)],\end{aligned} \qquad (7)$$

where the quantities can be obtained from standard thermochemical tables.[15] The temperature dependent magnitudes of $\Delta\mu_{\rm O}$ are summarized in Table 1 for pressures corresponding to the SPS and QA experiments and at 1 atm pressure.

T (K)	$\Delta\mu_{\rm O}[T,p^0]$ (eV)	$\Delta\mu_{\rm O}[T,p^{\rm SPS}]$ (eV)	$\Delta\mu_{\rm O}[T,p^{\rm QA}]$ (eV)
600	-0.610	-1.067	-1.384
700	-0.730	-1.264	-1.633
800	-0.850	-1.460	-1.882

Table 1 The magnitudes of $\Delta\mu_{\rm O}$ are tabulated here at $T = 600$, 700, 800 K. Here p^o is 1 atm pressure. Note that the value of $\Delta\mu_{\rm O}[p^o]$ at any temperature can be evaluated from Eq.(6), Eq.(7) and from the thermochemical tables in Ref. 15.

To evaluate the concentration of defects, $c_{\mathrm{D}^{(q)}}$, in a system, we first assume that we are in the dilute limit of defect concentrations, i.e. the amount of defects in the host is small enough for the electronic structure of the defected super-lattice to be approximated with that of the pristine host. Therefore, the expression resulting from conservation of charge is,

$$n_e - n_h = \sum_{\rm D} q c_{\mathrm{D}^{(q)}}, \qquad (8)$$

$$n_e = \int_{\varepsilon_{\rm CBM}}^{\infty} n(\varepsilon) f(\varepsilon;\mu_e)\,d\varepsilon\ ,\ n_h = \int_{-\infty}^{\varepsilon_{\rm VBM}} n(\varepsilon)[1 - f(\varepsilon;\mu_e)]\,d\varepsilon$$

where n_e and n_h are the number of electrons and holes. $\varepsilon_{\rm CBM}$ and $\varepsilon_{\rm VBM}$ are the conduction band minumum (CBM) and VBM respectively, $f(\varepsilon;\mu_e)$ is the Fermi-Dirac distribution and $n(\varepsilon)$ is the DFT density of States.

The equilibrium defect concentration, $c_{\mathrm{D}^{(q)}}$, at a particular temperature T can be obtained from Boltzmann's distribution as,

$$c_{\mathrm{D}^{(q)}} = c_0\,\exp\left(\frac{-E_d(\mathrm{D}^{(q)})}{k_{\rm B}T}\right), \qquad (9)$$

where c_0 is the number of the possible defect sites, E_d is the defect formation energy obtained from Eq. (1) and $k_{\rm B}$ is the Boltzmann's constant. The three simultaneous equations, Eq. (1), Eq. (8) and Eq. (9) can be solved to obtain E_d, μ_e and $c_{\mathrm{D}^{(q)}}$ for a given temperature. In the present case E_d is temperature dependent indirectly through μ_e which is determined by the charge neutrality condition, Eq. (8) and directly through $\mu_{\rm O}$, Eq. (6), which makes the procedure to extract the concentration of defects slightly different from earlier works.[3,11,16,17]

The total-energies entering in Eq. (1), were evaluated using the VASP Density Functional Theory (DFT) code[18,19], with PBE functional and PAW basis set[20,21] having a plane-wave cut-off of 350 eV. Corrections to $E(\mathrm{D}^{(q)})$ for alignment of the valence bands were included. Also the spurious electrostatic self-interactions due to the finite size supercells were accounted for.[22] The self-consistent total energy DFT calculations for the defected supercells were done for charged states between -3 and +3. The structures were relaxed till the forces on each atoms were less than 10^{-3} eV/Å.

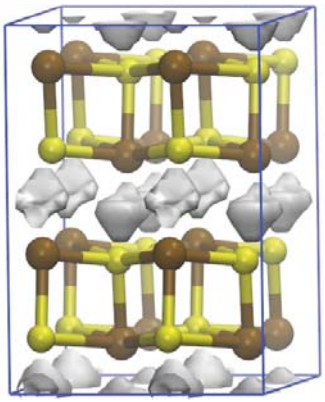

Fig. 2 Grey isosurfaces of the free volumes generated using Voronoi-interpolation method. Here Sn atoms are shown in brown and S atoms in yellow.

When studying the interstitial defects, we furthermore face the challenge of finding the most stable position for the defect. Intuitively, one would expect these positions to be found where there are free volumes available in the crystal. We therefore mapped out the Voronoi volumes of the cell to identify the positions with free volume. These are shown in Fig. 2 as the grey isosurfaces, which, as expected, are located, in between the Sn-S layers. We tested several other positions including positions within the SnS layers and indeed found that $\mathrm{D_{Int}}$ at the free volumes in between Sn-S layers had the lowest defect formation energy. This was true for D=Li, Ag and Cu.

3 Results and discussion

3.1 Coupled defect complexes

Fig. 3 shows the defect formation energies evaluated in the S rich conditions, as a function of μ_e. In this work, our definition of coupled defect is a complex of two distinct point defects with next nearest neighbor distances. We obtained that coupled defects of the form $\mathrm{D_{Sn}}$+$\mathrm{D_{Int}}$ has the lowest binding energy in comparision to all the other possible coupled defect permutations.

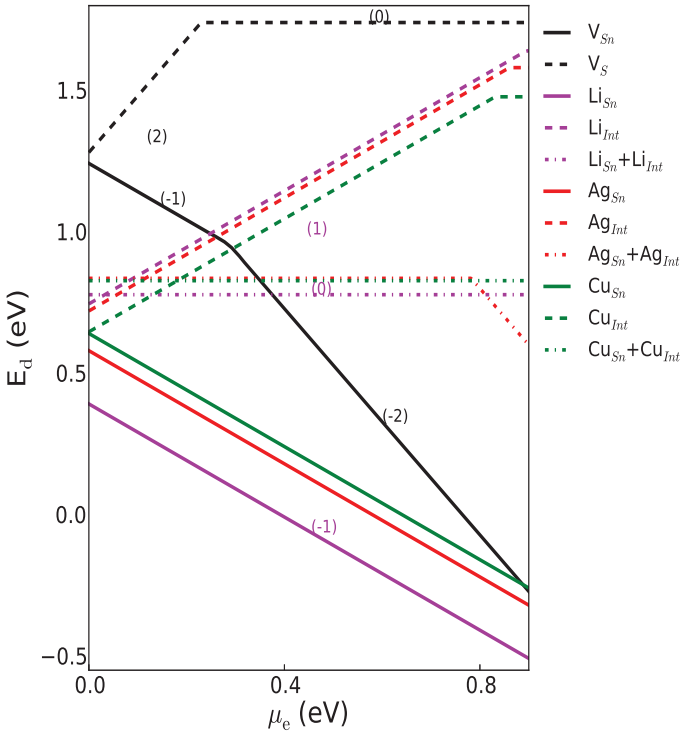

Fig. 3 The defect energy of the relevant uncoupled substitutional and intrinsic defects together with the coupled defects for Li, Ag and Cu, are shown as a function of chemical potential of the electron reservoir μ_e. The graph is shown for S rich conditions.

We observe that close to the VBM, all the coupled defects have higher formation energies in comparision to any of the relevant isolated defects. Taking Li doping at 800 K, which is approximately the temperature at which SnS is grown in the SPS experiments, the electron chemical potential takes the value $\mu_e = -0.04$ eV. The defect energies for the charged defects then have the following magnitudes, $E_\mathrm{d}(\mathrm{Li}_\mathrm{Sn}^{(-1)}, \mu_e) = 0.41$ eV and $E_\mathrm{d}(\mathrm{Li}_\mathrm{Int}^{(+1)}, \mu_e) = 0.73$ eV. The uncharged coupled defect energy is unaffected by μ_e and is $E_\mathrm{d}(\mathrm{Li_{Sn}} + \mathrm{Li_{Int}}) = 0.78$ eV. Dropping the charge and μ_e indices, the binding energy at 800 K of the coupled defect is

$$E_b = E_\mathrm{d}(\mathrm{Li_{Sn}}) + E_\mathrm{d}(\mathrm{Li_{Int}}) - E_\mathrm{d}(\mathrm{Li_{Sn}} + \mathrm{Li_{Int}}) = 0.36\ \mathrm{eV} \quad (10)$$

Thus the formation of complexes is energetically favorable compared to the two isolated $\mathrm{Li_{Sn}}$ and $\mathrm{Li_{Int}}$ defects. However, the positive binding energy does not mean that a $\mathrm{Li_{Sn}} + \mathrm{Li_{Int}}$ complex will form.[11] Defect complexes can form in two ways. One mechanism would require the $\mathrm{Li_{Int}}$ to diffuse to the $\mathrm{Li_{Sn}}$.

However, due to the relatively high $E_d(\mathrm{Li_{Int}})$, the concentration of such interstitial defects will be about 30 times less than that of $\mathrm{Li_{Sn}}$ at a growth temperature of 800 K. It is thus unlikely that diffusion of interstitial defects will strongly influence the carrier concentration. A further possibility would be the diffusion of substitutional defects. If two substitutional defects rearrange to form a coupled defect they would gain about 0.04 eV. However, a substitutional defect would first have to move to an interstitial position, before it can form a coupled defect. It would therefore have to overcome a barrier of at least $E_\mathrm{d}(\mathrm{Li_{Int}})+E_\mathrm{d}(\mathrm{V_{Sn}})-E_\mathrm{d}(\mathrm{Li_{Sn}})$ making it improbable for that kind of rearrangement to occur in a considerable quantity. Moreover, the probability that a considerable amount of defects form close to each other just by chance can also be ruled out by combinatorial considerations, which is in the spirit of the dilute limit.[11] Similar inferences were also be drawn for coupled defects in SnS doped with Li^+, Ag^+ and Cu^+. Thus, it seems unlikely that coupled defects form in a quantity, that affects the carrier concentration in an unfavorable way.

3.2 Oxidation of the dopant

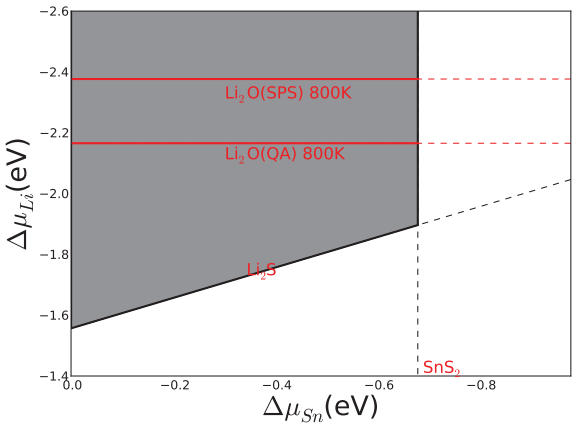

Fig. 4 Chemical potential limits for Li doping of SnS. The grey areas in the graph indicate the corresponding chemical potentials for $\Delta\mu_\mathrm{Li}$ and $\Delta\mu_\mathrm{Sn}$ that permit doping of SnS. The analogous competing phases are also labeled. The $\Delta\mu_\mathrm{Li}$ values corresponding to the formation of Li_2O in the QA and SPS experiments at $T = 800$ K, are also represented here in red horizontal lines.

In order to understand the role played by oxidation of Li on its ability to effectively dope the host semiconductor, we must compare the temperature dependent $\Delta\mu_\mathrm{Li}$ magnitude limited by the formation of Li_2O, Eq. (4), with its value determined by the formation of Li_2S, Eq. (5). Putting in the relevant numbers from Table 1 into Eq. (5), we obtained $\Delta\mu_\mathrm{Li}$ for the different pressures and temperatures as summarized in Table 2 and Fig. 4.

T (K)	$\Delta\mu_\mathrm{Li}[p^\mathrm{SPS}]$ (eV)	$\Delta\mu_\mathrm{Li}[p^\mathrm{QA}]$ (eV)	$\Delta\mu_\mathrm{Ag}[p^\mathrm{SPS}]$ (eV)	$\Delta\mu_\mathrm{Cu}[p^\mathrm{SPS}]$ (eV)
600	-2.573	-2.414	0.159	-0.841
700	-2.475	-2.290	0.356	-0.644
800	-2.377	-2.165	0.552	-0.448

Table 2 The limiting values of $\Delta\mu_\mathrm{D}$ due to the formation of oxides are shown for the pressures corresponding to the SPS and QA experiments, at three different temperatures. Note that 800K is taken as the approximate sample preparation temperature in the experiments, in the arguments of this section. All competing oxides were considered and the numbers are reported for the ones that were thermodynamically most stable at the relevant pressures, namely Li_2O, Ag_2O and CuO.

It is evident from Fig. 4 how the magnitude of $\Delta\mu_\mathrm{Li}$ is limited due to Li_2O formation at $T = 800$ K, even for the experiment done at QA pressures. Consequently, in this case the allowed $\Delta\mu_\mathrm{Li}$ to form $\mathrm{Li_{Sn}}$ defects will be pushed from -1.88 eV to -2.17 eV (for QA experiment) despite the UHV conditions and high temperature. In terms of the defect energy, in Fig. 3, it is clear that this would raise $E_d(\mathrm{Li_{Sn}})$ above that of $E_d(\mathrm{Ag_{Sn}})$, resulting in a lower carrier concentration of free holes. This argument is further supported in Fig. 5, where we compare dependence of the concentration of $\mathrm{Li_{Sn}}$ when no oxide formation is taken into account to when Li_2O formation is considered. Note that for both pressures, even for the QA experiment which was done under UHV conditions, the concentration of $\mathrm{Li_{Sn}}$ defects is greatly reduced from its original value. This is in agreement with the experiments, i.e. poor carrier concentration and high resistivity of Li^+ doped SnS. Due to oxidation of the dopant, there will be an unavailability of Li^+ to form the $\mathrm{Li_{Sn}}$ substitutional defect, thereby greatly reducing its concentration. Since the concentration of $\mathrm{Li_{Sn}}$ defects is directly proportional to the number of free holes in the $p-$doped system, the measured resistivity increases and thus the PF decreases. Note that we considered the oxidation of Li dopant into Li_2O because we found that it was the oxide which imposes the strictest limit on $\Delta\mu_\mathrm{Li}$.

To investigate the $\Delta\mu_\mathrm{Ag}$ range, we employed the same procedure as above. We first explored the oxidation of Ag under SPS pressures, as it is most likely that silver will get oxidized at this higher pressure (in comparision to QA). Table 2 contains the temperature dependent values of $\Delta\mu_\mathrm{Ag}$ required to form the silver oxides at SPS pressures. The positive values for $\Delta\mu_\mathrm{Ag}$ essentially confirm that the Ag^+ doping of SnS host will be resistant to oxidation. This is because for effective doping, an additional condition of $\Delta\mu_\mathrm{Ag} < 0$ is quintessential to prevent the precipitation of Ag (see Fig. 3 of Ref. 3). Consequently, in Fig. 5 we also observe that the $\mathrm{Ag_{Sn}}$ defect concentrations are unaffected by oxide formation for $T > 600$ K.

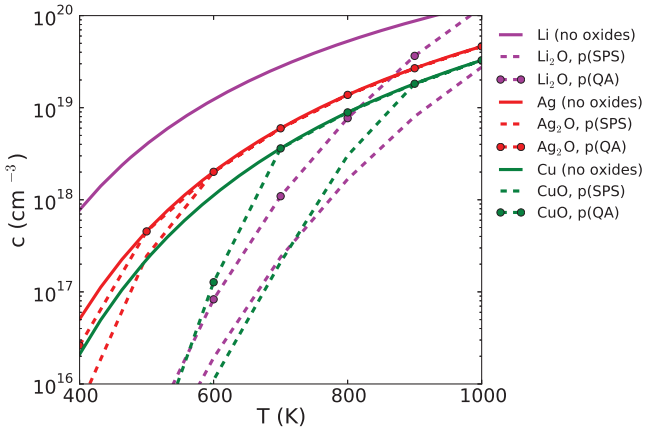

Fig. 5 The concentrations of Li_{Sn}, Ag_{Sn} and Cu_{Sn} defects as a function of growth temperature in doped SnS. The scenarios when no oxidation is taken into account (in bold lines) and when the oxidation of dopant D is considered under SPS (in dashed lines) and QA(in dotted dashed line) conditions are shown. The same color coding as Fig. 3 is used.

We finally considered Cu^+ as a potential dopant to produce the $p-$type behavior in SnS. The last column in Table 2 summarizes the temperature dependent $\Delta\mu_{Cu}[p^{SPS}]$ values that would result in the formation of copper oxides. Noting that for Cu^+ to effectively dope SnS in sulphur rich growth conditions, a condition of $\Delta\mu_{Cu} < -0.3$ eV must be satisfied. This limit is set due to the existence of a stable ternary competing phase Cu_2SnS_3, under these conditions[3]. Therefore the computed values of $\Delta\mu_{Cu}[p^{SPS}]$ in Table 2 suggest that the doping of SnS host with Cu^+ at $T = 800$ K would also be some what limited by the oxidation of the dopant. In Fig. 5 we also show the concentration of Cu_{Sn} defect as a function of temperature. For the scenario of Cu^+ doping of SnS, when oxidation of Cu is not taken into account, Cu_{Sn} defect concentration is slightly above $n = 10^{18}$ cm^{-3}, for the temperature range $T = 600 - 800$ K. For the QA experiment, the concentration of Cu_{Sn} defects will be unaffected by oxidation for $T \geq 700$ K. However, for the SPS experiment Cu_{Sn} defect concentration up to $T = 800$K is rapidly reduced. In general, we observe that for Cu^+ doped SnS in Fig. 5, we obtain lower hole concentrations in comparision to that achieved with Ag^+ doped SnS.

4 Conclusions

Through a combined experimental and theoretical effort, we have investigated in detail the $p-$doping of SnS thermoelectric with monovalent cations. In particular, we have explored the factors that would inhibit substitutional Sn doping and lead to low hole carrier concentrations and thereby high resistivities. This work was motivated by our measurements on Li^+ doped SnS which resulted in $\rho > 121$ mΩcm, while Ag doped SnS that resulted in $\rho = 38$ mΩcm. First principles defect energy studies had suggested both these monovalent cations should be soluble in the host semiconductor. We wanted to investigate the origin of this apparent disagreement between theory and experiment, especially since for Ag^+ doping of SnS we observed that theory leads to a fairly accurate estimation of the carrier concentration and thermoelectric properties[3,8].

To search for explanations for our experimental observations, firstly we investigated the effect of coupled defect complexes in reducing the itinerant hole concentrations. We have concluded that in general coupled defects are thermodynamically unfavorable in comparison to the individual point defects. Subsequently we explored the possibility of oxidation of the dopants as the cause to inhibit the hole concentrations. Indeed, we observed that for Li^+ doped SnS, Li_2O formation drastically reduced the concentration of free carriers. Our work suggest that this holds true even for the UHV experiment done at high temperatures. On the other hand we could quantitatively ascertain that for $T > 600$ K, and even for experiments done at higher pressures, oxidation of Ag will not affect its solubility in SnS.

While ab-initio defect thermodynamics is emerging as a very powerfull method for understanding and optimizing the carrier concentration in thermoelectrics,[3,10,17,23] the present work highlights the importance of considering the effect of oxidation. Furthermore, this paper also supports that for Ag^+ doped SnS, the doping is robust and resistant to oxidation in addition to the resultant thermoelectric exhibiting high power factors.

References

1 D. Spitzer, *J. Phys. Chem. Solids*, 1970, **31**, 19 – 40.
2 D. Parker and D. J. Singh, *Journal of Applied Physics*, 2010, **108**, 083712.
3 C. Bera, S. Jacob, I. Opahle, N. S. H. Gunda, R. Chmielowski, G. Dennler and G. K. H. Madsen, *Phys. Chem. Chem. Phys.*, 2014, **16**, 19894–19899.
4 M. M. Nassary and et al, *J. Alloy and Comp.*, 2005, **398**, 21.
5 W. Albers, C. Haas, H. J. Vink and J. D. Wasscher, *J Appl. Phys.*, 1961, **32**, 2220.
6 H. Noguchi, A. Setiyadi, H. Tanamura, T. Nagatomo and O. Omoto, *Solar Energy Materials and Solar Cells*, 1994, **35**, 325–331.
7 K. Ramakrishna Reddy, N. Koteswara Reddy and R. Miles, *Solar Energy Materials and Solar Cells*, 2006, **90**, 3041–3046.
8 Q. Tan, L.-D. Zhao, J.-F. Li, C.-F. Wu, T.-R. Wei, Z.-B. Xing and M. G. Kanatzidis, *J. Mater. Chem. A*, 2014, **2**, 17302–17306.
9 M. G. Wardle, J. P. Goss and P. R. Briddon, *Phys. Rev. B*, 2005, **71**, 155205.
10 C.-H. Park and Y.-S. Kim, *Phys. Rev. B*, 2010, **81**, 085206.
11 C. G. Van de Walle and J. Neugebauer, *Journal of Applied Physics*, 2004, **95**, 3851.
12 K. Reuter and M. Scheffler, *Phys. Rev. B*, 2001, **65**, 035406.
13 B. Meyer, *Phys. Rev. B*, 2004, **69**, 045416.

14 M. Finnis, A. Lozovoi and A. Alavi, *Annual Rev. Mater. Res.*, 2005, **35**, 167–207.
15 D. Stull and H. Prophet, *US National Bureau of Standards, Washington DC*, 1971.
16 D. Åberg, P. Erhart, A. J. Williamson and V. Lordi, *Phys. Rev. B*, 2008, **77**, 165206.
17 L. Bjerg, G. K. H. Madsen and B. B. Iversen, *Chem. Mat.*, 2012, **24**, 2711–2116.
18 G. Kresse and J. Hafner, *Phys. Rev. B*, 1994, **49**, 14251.
19 G. Kresse and J. Furthmüller, *Phys. Rev. B*, 1996, **54**, 11169–11186.
20 P. E. Blöchl, *Phys. Rev. B*, 1994, **50**, 17953–17979.
21 G. Kresse and D. Joubert, *Physical Review B*, 1999, **59**, 1758–1775.
22 G. Makov and M. C. Payne, *Physical Review B*, 1995, **51**, 4014–4022.
23 G. S. Pomrehn, A. Zevalkink, W. G. Zeier, A. van de Walle and G. J. Snyder, *Angew. Chem. Int. Edit.*, 2014, **53**, 3422–3426.